Analysis of flow induced crystallization through molecular stretch

Roberto Pantani*, Felice De Santis, Vito Speranza, Giuseppe Titomanlio

Dipartimento di Ingegneria Industriale, University of Salerno, Italy

Roberto Pantani

University of Salerno,

Department of Industrial Engineering,

Via Giovanni Paolo II, 132 - 84084 - Fisciano (SA)

E-mail: rpantani@unisa.it

Phone: +39 089 96 4141

Abstract

In this work, specific experiments on an isotactic polypropylene are carried out, aiming to investigate the flow induced crystallization and the final morphology. The viscoelastic nature of the polymer is described by a non-linear Maxwell model applied to the conformation tensor. Shear stress evolutions, recorded during step shear isothermal experiments, are satisfactory described considering the molecular stretch, i.e. the difference between the two main eigenvalues of the conformation tensor. In the general model, the effect of temperature, pressure, and crystallinity are taken into account. Furthermore, a modeling framework is proposed to describe flow-induced crystallization of isotactic polypropylene. The spherulitic growth rate is analyzed on the basis of a flow dependent equilibrium melting temperature, using the molecular stretch as the key parameter. A phenomenological correlation of the nucleation rate with growth rate is observed. By combining the morphological models, both for nucleation and growth rate, for flow induced crystallization is possible to explain the effect of shear rate and shearing times in different experimental results, and potentially in the simulation of polymer processing.

Keywords

Nucleation and growth rates; Shear Flow; Flow-induced crystallization

Introduction

Many characteristics of polymeric products are determined by morphology distribution induced by their manufacturing process [1, 2].

The evolution of morphology is determined by the thermomechanical history up to solidification [3, 4], which in polymer processing operations may take place at very high cooling rates and pressures and under the effect of flow. This framework is even more complex for thermoplastic materials like isotactic polypropylene, i-PP, in which different crystalline phases and different morphologies can coexist. Dominantly present in i-PP is typically the α-phase [5, 6], between three different ordered crystalline phases, formed at atmospheric pressure and low to moderate cooling rate.

Indeed, in the last decades, large interest was devoted by researchers to clarify main aspects of the effect of cooling rate, pressure and flow on morphology evolution of thermoplastic polymers [7-12].

Experimental observations were carried out by different research groups over the years, by using essentially two protocols: continuous flow, in which the material undergoes to deformation for most of the crystallinity evolution time [13, 14]; step shear flow, in which the deformation is imposed for a short time [15-18]. The latter protocol may separate the effects of flow on the molecular stretch from the effects of crystallization on the rheological behavior [19-21].

According to the current understanding, the effect of flow on crystallization may be schematized as follows:

i) there is a threshold below which morphology evolution keeps quiescent features;
ii) above such a threshold, nucleation density and growth rate are affected by the flow;
iii) above a second threshold, crystallization features change into fibrillar morphology and related fibrillar crystallization kinetics.

Furthermore, it is widely recognized that the effect of flow on crystallization kinetics has to be related to molecular stretch, whose evolution determines nucleation density and spherulitic growth rate and, thus, the evolution of morphology up to solidification. Indeed, the values of the thresholds identified above are normally related to the Weissenberg number [22] which, comparing the characteristic times of flow intensity and molecular relaxation, gives an idea of the capacity of flow to orient and stretch the macromolecules.

A literature survey of the current models for flow-induced crystallization (reviews are given by Pantani et al [7] and by Peters et al [22]) shows that in order to describe the enhancement of crystallization kinetics induced by flow it is necessary to model the effect of flow on molecular conformation (by means of a viscoelastic model) and the nucleation and growth of crystalline structures.

In this work, a model for the evolution of morphology during crystallization is proposed on the basis of the simple model of molecular stretch evolution reported in [7]. Furthermore, experiments of i-PP Flow Induced Crystallization are carried out in this work with the aim of characterizing the parameters of the model and comparing the model predictions with final solidification morphology.

Experimental

Material

The material adopted in this work was an i-PP (tradename of Moplen T30G, supplied by Montell). This resin is a general-purpose homopolymer for extrusion/molding applications, with a melt flow index equal to 3.6 (ASTM D1238/L). The molecular weight distribution was determined by a size exclusion chromatography as weight-average molar mass M_w of 376 kg mol^{-1}, polydispersity index M_w/M_n of 6.7, and meso pentads content 87.6%. The glass transition temperature (T_g) and melting temperature of Moplen T30G reported on the material datasheet are -15 °C and 166 °C, respectively. The rheology and the crystallization kinetics of the same resin were the focus of several studies [23-29].

The steady state viscosity of the polymer melt was well described by a Cross model [7].

$$\eta\left(T,P,\chi,\dot{\gamma}\right)=\frac{\eta_0\alpha_v\left(T,P,\chi\right)}{1+C\left[\eta_0\alpha_v\left(T,P,\chi\right)\dot{\gamma}\right]^{1-r}} \tag{1}$$

where $\dot{\gamma}$ is the shear rate and the shift factor, $\alpha_v\left(T,P,\chi\right)$, which takes into account the changes due to temperature, T, pressure, P, and relative crystallinity degree [21], χ, was given by a modified WLF equation,

$$\alpha_v\left(T,P,\chi\right)=\exp\left[-\frac{D_1\left(T-T_0\right)-D_3P}{D_2+\left(T-T_0\right)}+D_4\chi^{D_5}\right] \tag{2}$$

The parameters to be used in Eqs. 1 and 2 are listed in Table 1.

Table 1. Parameters adopted to describe viscosity of i-PP resin T30G.

parameter	value	parameter	value
D_1	4.006	η_0 [Pa s]	6387
D_2 [K]	301.4	C	0.0023
D_3 [K bar^{-1}]	0.6811	r	0.34
D_4	180	T_0 [K]	503
D_5	2		

The material was characterized in the literature for quiescent crystallization (nucleation density, growth rate, and mesomorphic crystallization rate) also under very high cooling rates and pressure [7-9, 30]. Under quiescent conditions, the nucleation was found to have a heterogeneous character; indeed, the nucleation density was verified to be a function of temperature only [8, 31].

Methods

The effect of flow on the spherulitic crystallization of the material was assessed in the literature [7]. In particular, in a recent paper [32], step shear tests were conducted in the Linkam shearing device (parallel plates configuration) imposing a given plate rotation speed for a given time at the temperature of 140 °C. Due to the geometrical configuration of the system, since in plate-plate configuration the gap between the top and the bottom plates is constant, the shear rate varies linearly with radius, so there is a radial distribution of the shear rate. Shear rates in the range 0-8 s^{-1} were imposed to each sample, for shearing times chosen in the range 10-40 s [32]. The distribution of diameters of spherulites inside the samples was then characterized by means of optical microscopy. Those results [32] will be used in this work to validate the model for flow-induced crystallization.

Some data of morphology distribution in samples subjected to shear flow were also collected in this work. In particular, a Multipass Rheometer (MPR) [10] was adopted as a device able to impose a given shearing history to the samples. This MPR was developed at the Technical University of Eindhoven and was equipped with a slit geometry 120 mm long, 6 mm wide and 1.5 mm thick. The thermal history experienced by the material is reported in Fig. 1. The material was held above its equilibrium melting temperature at 220 °C for 10 min, in order to erase the effects of previous thermomechanical history. Subsequently, it was cooled down, with a cooling rate of 10 °C min^{-1}, to the test temperature, T_s=140 °C, at which it was kept for 1 h. The material was then cooled to room temperature, which was reached about 5 min after the cooling start. Also in this case, the flow was applied soon after reaching 140 °C and according to a step-shear protocol, also represented in Fig. 1: after about 2 s from the start of the isothermal step, a constant velocity was imposed to the pistons and thus the material inside the slit was forced to reach a constant average velocity, v_{av}=1 mm s^{-1}. This velocity was held for shearing times, t_{shear}, of 1 s and 20 s.

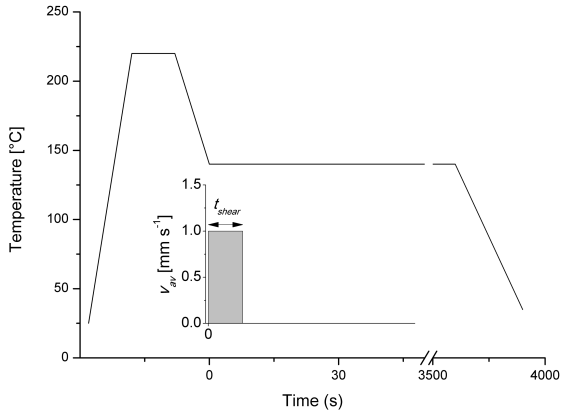

Fig. 1. Schematics diagram for temperature and shear protocols adopted with Multi Pass Rheometer (MPR).

The samples solidified inside the MPR were cut by a microtome in order to obtain thin (20 μm) slices in-plane flow (parallel to the slice plane) at known distances from the skin. These slices were then characterized via polarized optical light microscopy.

Since the model for flow-induced crystallization presented in this work relies on the assessment of molecular stretch, it was necessary to validate the viscoelastic parameters of the material. To this goal, some data of shear stress in unsteady conditions were collected in this work. The device used is an ARES (Rheometrics) rheometer with a cone-plate configuration at the constant temperature of 140 °C. The tests were carried out according to the protocol reported in Fig. 2: a shear rate of 0.01 s^{-1} was kept constant until a plateau in the measured shear stress was measured; the value of shear rate was then increased to 0.81 s^{-1} or to 0.27 s^{-1} or to 0.03 s^{-1} and kept constant for 60 s; the shear rate was decreased again to 0.01 s^{-1}. During the whole test, the shear stress was measured and recorded. The tests were fast enough to avoid any significant crystallization during the time needed for measurements.

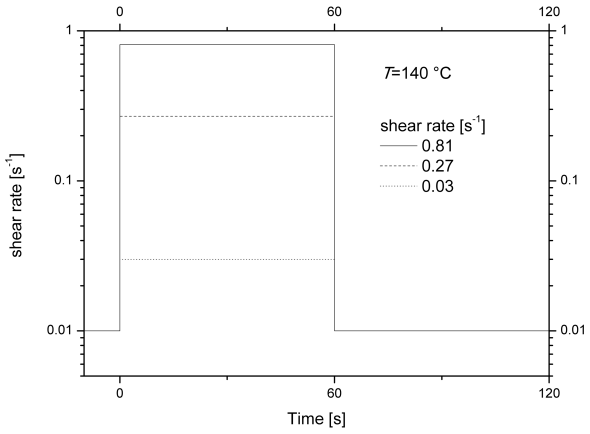

Fig. 2. Schematics diagram for step shear experiments performed with the ARES rheometer.

Results

Experimental results obtained by MPR

Some micrographs of the samples solidified in the MPR are reported in Fig. 3. The samples present spherulitic morphology, also in the layers very close to the skin. For all the samples it is clear that the spherulite dimensions increase on increasing the distance from the skin.

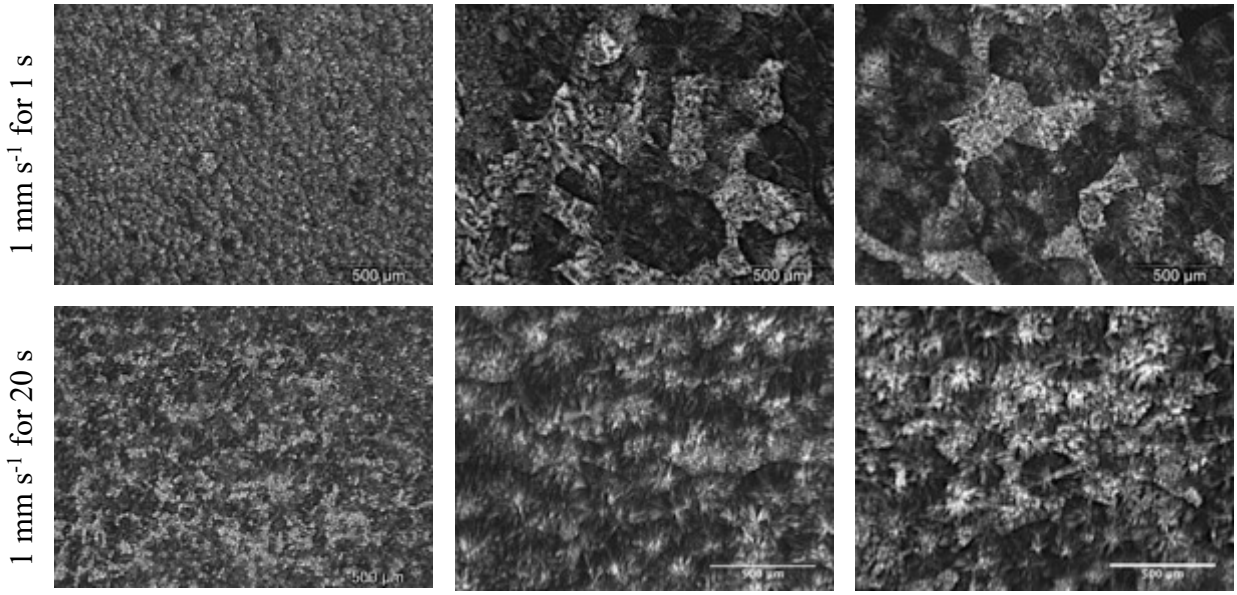

Fig. 3. Micrographs of the samples solidified in the MPR at 140 °C, at three distances from the midplane, applying constant average velocity, v_{av}=1 mm s^{-1}, for shearing times, t_{shear}, of 1 s and 20 s.

It is worth mentioning that, in the condition analyzed in this work, it cannot be excluded that some β crystalline form can be formed, together with the well recognizable α spherulites. Indeed, some brighter structures can be noticed in the pictures taken closer to the sample skin, which could be indeed β spherulites. These structures present about the same characteristic dimensions as the α spherulites, suggesting a similar crystallization kinetics in the conditions analyzed in this work. The possible formation of other crystalline phases will be considered in the following. The dimensions of the spherulites are reported in Fig. 4. At the midplane, both the samples present the same average dimensions for the spherulites (a radius of about 130 µm). On moving toward the skin, the sample which experienced the shortest shearing time (1 s) presents more homogeneous spherulite dimensions, which reduce significantly just very close to the skin. The sample which experienced the longest shearing time (20 s) presents that reduction at a distance of about 150 µm from the midplane. At the skin, the spherulite dimensions appear to be about the same for both samples, namely a radius of about 40 µm.

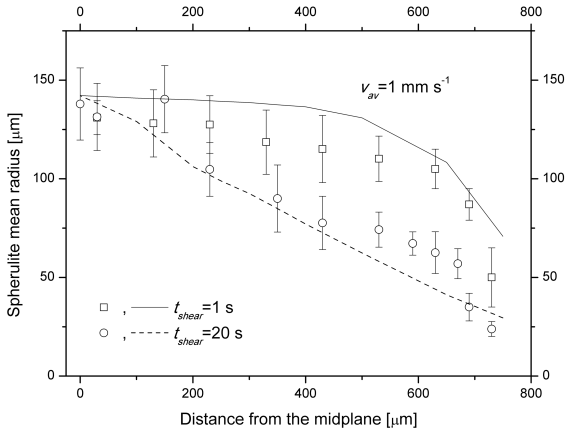

Fig. 4. Spherulite mean radius, for samples solidified in MPR at 140 °C, as a function of the distance from the midplane applying constant average velocity, and v_{av}=1 mm s^{-1}, for shearing times, t_{shear}, of 1 s and 20 s. Symbols and lines are the experimental values and the model predictions, respectively.

Model for molecular orientation

In this work, a non-linear formulation of a Maxwell model applied on the conformation tensor $\underset{\sim}{\underset{\sim}{A}}$ [7, 10, 33, 34] was adopted to describe the viscoelastic nature of the polymer. According to this model [35], the constitutive equation can be written as

$$\frac{D}{Dt}\underset{\sim}{\underset{\sim}{A}}-\left(\nabla\underset{\sim}{v}\right)^{T}\cdot\underset{\sim}{\underset{\sim}{A}}-\underset{\sim}{\underset{\sim}{A}}\cdot\left(\nabla\underset{\sim}{v}\right)=-\frac{1}{\lambda}\underset{\sim}{\underset{\sim}{A}}+\left(\nabla\underset{\sim}{v}\right)+\left(\nabla\underset{\sim}{v}\right)^{T} \tag{3}$$

in which $\underset{\sim}{\underset{\sim}{A}}$ is a tensor representing the deformation of the dumbbells with respect to the equilibrium state:

$$\underset{\sim}{\underset{\sim}{A}}=3\frac{\left\langle\tilde{R}\tilde{R}\right\rangle-\left\langle\tilde{R}\tilde{R}\right\rangle_{0}}{\left\langle R_{0}^{2}\right\rangle} \tag{4}$$

$\underset{\sim}{v}$ is the velocity vector and λ is the relaxation time.

The stress tensor $\underset{\sim}{\underset{\sim}{\tau}}$ is proportional to the tensor $\underset{\sim}{\underset{\sim}{A}}$ through the shear modulus G_S

$$\underset{\sim}{\underset{\sim}{\tau}}=G_{S}\underset{\sim}{\underset{\sim}{A}} \tag{5}$$

The difference between the two main eigenvalues of the tensor $\underset{\sim}{\underset{\sim}{A}}$, named Δ in this work, was assumed as a measure of the elongation of the dumbbell population [7, 10]. In simple shear flow, where "*x*" is the flow direction, "*y*" is the thickness direction, going from the midplane to the wall, Δ can be written as

$$\Delta=\sqrt{A_{xx}{}^{2}+4A_{yx}{}^{2}} \tag{6}$$

and under steady state conditions, $A_{xx} = 2\left(\dot{\gamma}\lambda\right)^2$, $A_{yx} = \left(\dot{\gamma}\lambda\right)$, where $\dot{\gamma}$ is the shear rate defined as

$$\dot{\gamma}\left(y,t\right) = \left|\frac{\partial}{\partial y} v_x\left(y,t\right)\right| = -\frac{\partial}{\partial y} v_x\left(y,t\right) \tag{7}$$

Thus in simple shear Δ becomes

$$\Delta = 2\left(\dot{\gamma}\lambda\right)\sqrt{1+\left(\dot{\gamma}\lambda\right)^2} \tag{8}$$

The relaxation time was found to be well described by the following function of Δ [36]

$$\lambda\left(T,P,\chi,\Delta\right) = \frac{\lambda_0 \alpha_t\left(T,P,\chi\right)}{\left[1+\left(a\Delta\right)^b\right]^c} \tag{9}$$

in which λ_0, a, b, and c are constants. The shift factor α_t takes into account the effect of temperature, pressure, and crystallinity and can be expressed as

$$\alpha_t\left(T,P,\chi\right) = \exp\left[-\frac{C_1\left(T-T_0\right)-C_3 P}{C_2+\left(T-T_0\right)} + C_4 \chi^{C_5}\right] \tag{10}$$

Also, the viscosity can be expressed in terms of Δ as follows

$$\eta\left(T,P,\chi,\Delta\right) = \frac{\eta_0 \alpha_v\left(T,P,\chi\right)}{\left[1+\left(d\Delta\right)^e\right]^f} \tag{11}$$

where shift factor, α_v, is given by Eq. 2.

Considering that the shear modulus G_S is given by the ratio between viscosity and relaxation time, it could be described as a function of Δ by the following equation

$$G_S\left(T,P,\chi,\Delta\right) = G_{S0}\frac{\alpha_t\left(T,P,\chi\right)}{\alpha_v\left(T,P,\chi\right)}\frac{\left[1+\left(d\Delta\right)^e\right]^f}{\left[1+\left(a\Delta\right)^b\right]^c} \tag{12}$$

The parameters to be adopted in the Eqs. from 9 to 12 were obtained from rheological data collected in dynamic mode, following the procedure reported in the literature [7, 21, 36] and are reported in Table 2.

Table 2. Parameters adopted to describe viscoelastic behavior and shear modulus of i-PP resin T30G.

parameter	value	parameter	value
C_1	5.756	C_5	2
C_2 [K]	301.4	λ_0 [s]	14
C_3 [K bar^{-1}]	0.9786	T_0 [K]	503
C_4	180	G_{S0} [Pa]	456.2
d	0.83	a	3.8
e	2.3	b	2.2
f	0.67	c	1

In order to validate the model predictions during unsteady conditions, the shear stress evolutions recorded during and after the shear steps, performed with the ARES rheometer at the temperature of 140 °C were compared in Fig. 5 with the predictions of the model described by Eqs. 3-12. It appears that, except for the small stress overshoot shown by the data at large shear rates, the model satisfactory describes all features of experimental data. In particular: the stress levels obtained by the model practically coincide with the experimental values, the time for stress build up decreases with the stress level similarly for the experimental results and predictions of the model; also the stress relaxation after each shear rate step is satisfactorily described by the model.

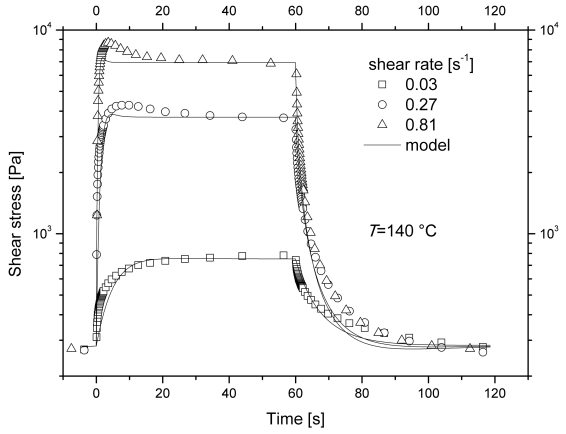

Fig. 5. Shear stress evolutions during and after step shear experiments at 140 °C with the ARES rheometer: experimental values (reported as symbols) and model predictions (reported as lines).

Discussion

Effect of flow on growth rate

The main assumption of the model for flow-induced crystallization, adopted in this work, is that the increase in both the growth and the nucleation rates are related to molecular strain [37, 38].

The effect of flow upon spherulitic growth rate was analyzed on the basis of a flow dependent equilibrium melting temperature, T_m^0, which is a parameter of the Hoffman-Lauritzen model describing the growth rate [32, 37].

$$G(T) = G_0 \exp\left[-\frac{U/R}{T - T_\infty}\right] \exp\left[-\frac{K_g\left(T + T_m^0\right)}{2T^2\left(T_m^0 - T\right)}\right] \tag{13}$$

The parameters to be adopted in Eq. 13 for i-PP are reported in Table 3.

Table 3. Values of the parameters adopted to describe the experimental data of quiescent spherulitic growth rate as identified in a previous work [37].

	G_0 [μm s^{-1}]	U/R [K]	K_g [K^2]	T_∞ [°C]
Regime III, T<137 °C	2.9 10^{10}	751.6	534858	-37.2
Regime II, T>137 °C	1.7 10^{5}	751.6	267429	-37.2

In other words Eq. 13 was assumed to be valid also under flow conditions, limiting the effect of flow just on the equilibrium melting temperature T_m^0, which under flow replaces the quiescent value T_{mq}^0. In a previous work [32] a correlation was found between T_m^0 and the steady state shear rate $\dot{\gamma}$ experienced by the samples. The flow induced equilibrium melting temperature T_m^0 can be associated to the molecular strain parameter Δ, which in turn is linked to the shear rate $\dot{\gamma}$ as specified by Eq. 8. The results are reported in Fig. 6 and identify the correlation between T_m^0 and Δ.

Although the correlation of Fig. 6 was obtained by experiments performed under step and steady state shear conditions, it identifies a relation between T_m^0 and Δ which has a general validity for the material: namely, once Δ is known, whatever the condition it refers to, it can be adopted to evaluate T_m^0 (and thus the growth rate through Eq. 13).

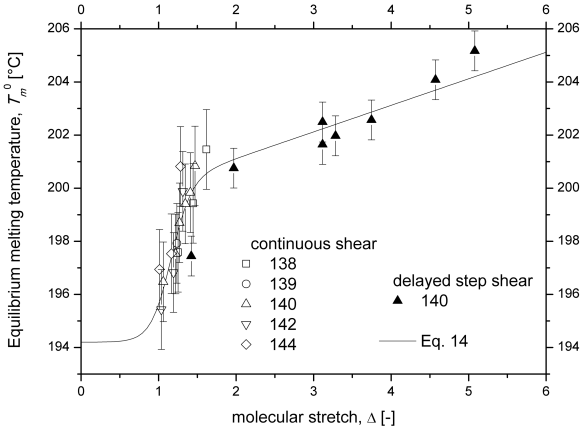

Fig. 6 Equilibrium melting temperature T_m^0 vs molecular stretch Δ: experimental values (continuous shear as open symbols [32], delayed step shear as solid symbols [37]) and fitting by Eq. 14 (reported as a line). Few literature data, collected with continuous shear protocol [37], were neglected considering the delayed step shear protocol more consistent [32].

As shown in Fig. 6, the following equation,

$$T_m^0(\Delta) - T_{mq}^0 = \frac{1}{2}\left[\tanh\left(\frac{\Delta - A_1}{A_2}\right) + 1\right](A_3\Delta + A_4) \qquad (14)$$

with the values of the parameters reported in Table 4, reproduces the dependence of T_m^0 upon Δ shown by the data.

Table 4. Parameters used in Eq. 14 to describe the dependence of T_m^0 upon Δ.

T_{mq}^0 [°C]	194
A_1	1.15
A_2	0.26
A_3 [K]	1
A_4 [K]	4.92

Effect of flow on nucleation rate and the crystallization kinetics model

Under quiescent conditions, instantaneous nucleation was predominant in the material adopted in this work [8]: namely, nucleation density was just dependent on temperature. An additional effect to the nucleation density was observed and measured under steady shear conditions [37, 39], due to flow induced nucleation rate.

A correlation among the excess of growth rate (with respect to quiescent conditions) and the nucleation rate under the same conditions (of shear rate and temperature) was identified in a previous work [32]. The existence of such a correlation between growth rate and nucleation rate is consistent with the fact that also nucleation rate is usually described by Hoffman-Lauritzen equation. The curve, drawn among the data reported in Fig. 7, is described by Eq. 15.

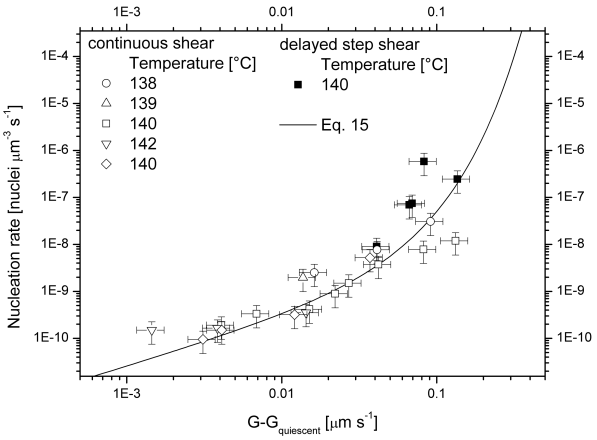

Fig. 7. Nucleation rate versus excess growth rate for i-PP under several temperature and shear rate conditions: experimental values (continuous shear as open symbols [32], delayed step shear as solid symbols [37]) and fitting by Eq. 15 (reported as a line).

$$\dot{N} = 2.5\times10^{-8}\left(G - G_{quiescent}\right)\exp\left[30\times\left(G - G_{quiescent}\right)\right] \tag{15}$$

On the basis of the knowledge of the local shear rate history, the evolution of Δ can be calculated by the viscoelastic model described above. This allows to calculate the time evolution of T_m^0 from Eq. 14 and thus the growth rate from Eq. 13. The correlation reported in Fig. 7, allows then to calculate the nucleation rate. The Avrami Kolmogorov's model can then be adopted to evaluate the evolution of relative crystallinity according to the equation

$$\frac{\partial \chi_\alpha}{\partial t} = \left(1-\chi\right)\frac{\partial k_\alpha}{\partial t} \tag{16}$$

where χ is the overall relative crystallinity degree (comprising all crystalline phases), χ_α is the relative crystallinity degree of the α phase and k_α is the volume fraction of the α phase if no impingement would occur and is given by:

$$k_\alpha = \frac{4\pi}{3}\int_{s=0}^{t}\frac{dN_\alpha(s)}{ds}\left(\int_{u=0}^{t} G(u)\,du\right)^3 ds \tag{17}$$

in which N_α is the total number of nuclei of the α phase, due to both the nucleation rate (as obtained from the correlation shown in Fig. 7) and to the heterogeneous nuclei, N_0, generated at the chosen temperature in the quiescent condition.

$$\frac{dN_\alpha}{dt} = \dot{N} + \frac{dN_0}{dt}\dot{T} \tag{18}$$

Following experimental evidence, the number of heterogeneous nucleation density N_0 was assumed to depend on the temperature according to an exponential function of the undercooling [7], so that in the isothermal experiments performed in this work the constant value N_0 (140 °C)= 8.3×10^{-8} nuclei μm^{-3} was adopted.

At each instant the number of active spherulites of α phase, N_a, was calculated as [8]

$$N_a = \int_{s=0}^{t} \frac{dN_\alpha(s)}{ds}\left(1-\chi(s)\right)ds \tag{19}$$

and the final average radius of the spherulites as [8]

$$\bar{R} = \sqrt[3]{3\chi_\alpha / 4\pi N_a} \tag{20}$$

If only α phase is present, χ_α in eq. 20 is equal to 1. If other crystalline phases are present the value of χ_α is obviously lower than 1 and a complete simulation of the crystallinity evolution of the other phases should be carried out in order to calculate this value. However, it could be noticed that, being the value of χ_α in a cube root, the presence of other crystalline phases up to 30% of the volume occupancy (namely with χ_α of about 0.7) would give rise to an average radius only 10% lower than that calculated considering the formation of α phase only (namely with χ_α equal to 1), which is well within the scatter of experimental data. In the following, therefore, the presence of other crystalline phases will be neglected in the calculation, with the warning that the predictions could be overestimated by about 10% especially at the highest shear rates, where some β phase could indeed form as suggested by Fig. 3.

Prediction of final morphology distribution in Linkam shearing experiments

Once the parameters of the viscoelastic model were determined, it was possible to calculate the evolution of the parameter Δ during the experiments carried out by the Linkam shearing cell. For those experiments, the shear rate is constant at each radial position during the shearing time, and it changes just with the radial position. In Fig. 8 the evolution of the parameter Δ (Fig. 8A) and of the relaxation time (Fig. 8B) is reported for the test carried out at 140 °C with a shearing time of 10 s and at two positions, where the shear rate was 2 and 5 s^{-1}, respectively.

For both shearing conditions as soon as shear is applied Δ, reported in Fig. 8A, undergoes to a rapid increase and as a consequence the relaxation time, reported in Fig. 8B, decreases. After shearing, Δ decreases and thus the relaxation time increases to the quiescent value again.

The maximum value of parameter Δ is larger for larger applied shear rates and the time needed to reach steady conditions reduces on increasing the shear rate, being of the

order of 1 s for both the shear rates considered.

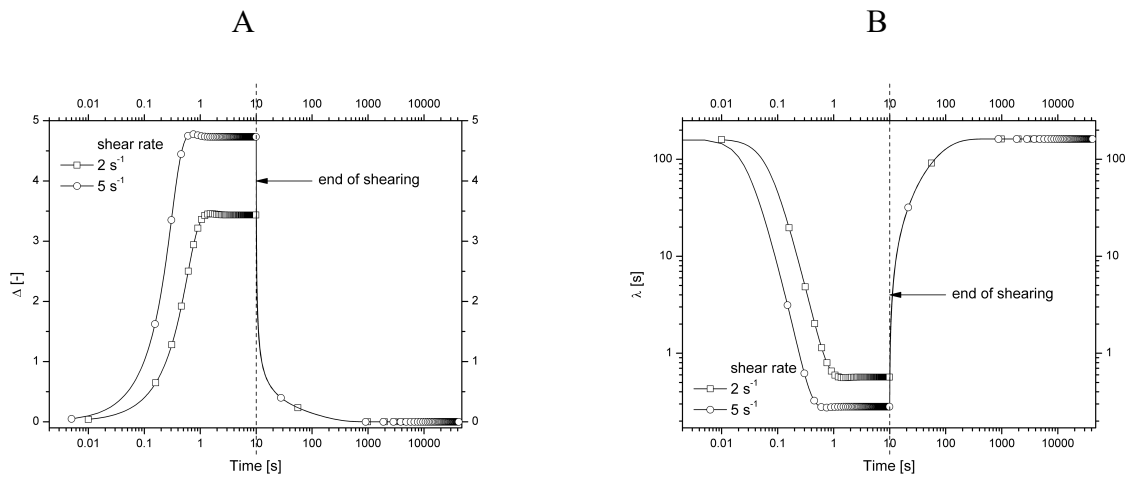

Fig. 8. Evolution of molecular stretching parameter Δ (A) and relaxation time (B) during and after the application of a step, for a shearing time of 10 s, at 140 °C with a shear rate of 2 and 5 s^{-1}.

According to the model described above, it was possible to calculate the evolution of the main morphological parameters during the tests carried out by the Linkam apparatus. As an example, in Fig. 9 we report the time evolution of the number of nuclei and of the overall relative crystallinity degree for the test conducted with a shearing time of 10 s at two radial positions, corresponding to the shear rates of 2 and 5 s^{-1}. At higher shear rates, the number of nuclei, which is initially equal to the predetermined value at the test temperature (140 °C), increases at shorter times and with a higher rate, so that it reaches a higher value at the end of the shearing. Afterward, it remains constant. It is noteworthy that the crystallization starts to increase at much longer times so that the two phenomena of nucleation and growth are essentially in series. Obviously, due to the much larger number of nuclei, the crystallinity degree increases much earlier at the positions which experienced a larger shear rate. This also means that, according to Eq. 19, all the nuclei are active.

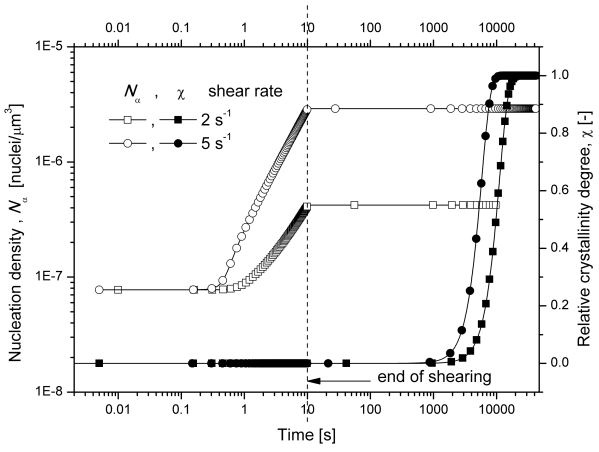

Fig. 9. Prediction of nucleation density and relative crystallinity evolution during and after the application of a step, for a shearing time of 10 s, at 140 °C with a shear rate of 2 and 5 s^{-1}.

The calculated final distributions of diameters inside the samples solidified inside the Linkam apparatus are compared with the experimental results in Fig. 10. It is clear that the calculations run very close to the data and reproduce correctly the effects of shear rate and shearing time.

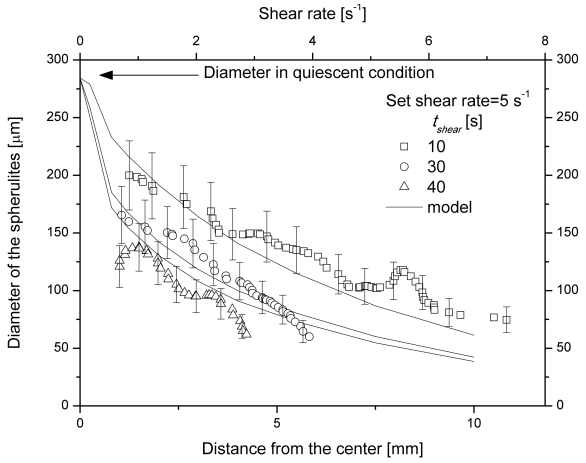

Fig. 10. Diameter as a function of the radial distribution of shear rate in the Linkam apparatus, with set shear rate 5 s^{-1}, shearing time 10, 30, and 40 s: symbols and lines are the experimental values [32] and the model predictions, respectively. The arrow on the top of the plots indicates the diameter reached by the spherulites in quiescent conditions, at 140 °C.

Prediction of final morphology distribution in MPR experiments

From the evolution of molecular stretching parameter Δ and relaxation time, shown in Fig. 8, it is clear that when the shear step is conducted for times of the order of 1 s, the viscoelastic nature of the polymer cannot be neglected even on the evolution of velocity profile.

The time evolution of the velocity profile was calculated by imposing the average velocity to be a constant, v_{av}, equal to that set by the MPR.

The adopted procedure is applied to the numerical solution of PDE, obtained in simple shear from the equation of motion in terms of stress:

$$\frac{\partial}{\partial x}\tau_{yx}(y,t) = -\frac{\partial}{\partial x}P(t) - \rho\frac{\partial}{\partial t}v_x(y,t) \tag{21}$$

in which τ_{yx} is obtained by applying Eq. 5 to the *yx*-component of the tensor $\underset{\sim}{A}$. In simple shear, the evolution of this component is given by

$$\frac{\partial A_{yx}}{\partial t} = \dot{\gamma} - \frac{A_{yx}}{\lambda} \tag{22}$$

In order to calculate the modulus G_S and the relaxation time, λ, is considered to be a function of molecular stretch, Δ. This requires the knowledge of the *xx*-component of the tensor A, which in simple shear is given by

$$\frac{\partial A_{xx}}{\partial t} = 2\dot{\gamma} A_{yx} - \frac{A_{xx}}{\lambda} \tag{23}$$

The solution procedure starts from a flat velocity profile (except at the walls where velocity is set to zero); calculates the time derivatives on the basis of the values of each variable at the previous time and, at each time, estimates the value of the pressure gradient $\partial P/\partial x$ which, following the previous equations, assures a velocity profile consistent with an average velocity equal to v_{av}.

In agreement with the observations described above, it was found that the time needed to reach the steady state velocity profile during the MPR experiments at 140 °C with an average velocity v_{av} = 1 mm s^{-1} (shear rates from 0 to 6 s^{-1}) was about 1 s. The evolution of velocity and shear rate as calculated by Eqs. 1-23 are reported in Fig. 11A and Fig. 11B, respectively.

A B

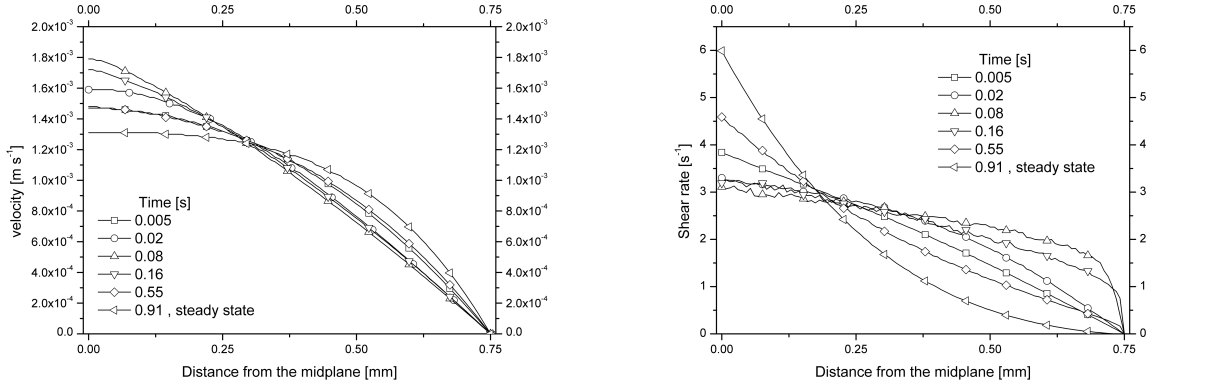

Fig. 11. The evolution of velocity (A) and shear rate (B), in MPR experiments at 140 °C with an average velocity v_{av} = 1 mm s^{-1}, as calculated by Eqs. 1-23.

The results of the simulations are compared with the experimental results of the final morphology of samples solidified inside the MPR in Fig. 4. Also in this case, despite the high complexity of the test, the effect of different shearing time, 1 s and 20 s respectively, and the distribution of spherulite dimension in the samples are correctly reproduced.

Conclusions

The effect of flow on the morphology evolution during crystallization of an iPP has been modeled.

The model describes the effect of flow on nucleation density and growth rate, which are combined according to Kolmogorov model. The effect of flow is lumped into a scalar invariant measure of the molecular stretch, obtained from the conformation tensor whose evolution is described by a not linear contravariant Maxwell equation; the non-linearity being described through a relaxation time in its turn function of the molecular stretch.

The effect of the stretch on growth rate is identified by means of optical microscopy observation during simple shear tests in rotational geometry. The growth rate was found to increase with the

molecular stretch, such an increase was ascribed to an increase of the undercooling due to the increase (by the effect of flow) of the equilibrium melting temperature which enters Hoffman-Lauritzen equation for the dependence of growth rate upon temperature. A correlation was identified between the stretch parameter and the equilibrium melting temperature.

The increase of nucleation density by the effect of flow was described by a nucleation rate, which also was found function of the molecular stretch and the data supported a correlation with the growth rate.

The results of the whole model nicely compare with experimental results of the final morphology of samples isothermally crystallized under the effect of shear flow. A comparison between model predictions and experimental data of morphology evolution during solidification at different temperatures could give interesting indications before adopting the model into the simulation of polymer processing.

References

1. Housmans J-W, Gahleitner M, Peters GW, and Meijer HE. Polymer 2009;50(10):2304-2319. doi:10.1016/j.polymer.2009.02.050
2. Caelers H, Govaert L, and Peters G. Polymer 2016;83:116-128. doi:10.1016/j.polymer.2015.12.001
3. Schrauwen B, Breemen Lv, Spoelstra A, Govaert L, Peters G, and Meijer H. Macromolecules 2004;37(23):8618-8633. doi:10.1021/ma048884k
4. Sorrentino A, De Santis F, and Titomanlio G. Polymer crystallization under high cooling rate and pressure: a step towards polymer processing conditions. Progress in Understanding of Polymer Crystallization: Springer, 2007. pp. 329-344. doi:10.1007/3-540-47307-6_16
5. Roozemond PC, van Erp TB, and Peters GW. Polymer 2016;89:69-80. doi:10.1016/j.polymer.2016.01.032
6. Brucato V, De Santis F, Lamberti G, and Titomanlio G. Polymer Bulletin 2002;48(2):207-212. doi:10.1007/s00289-002-0020-4
7. Pantani R, Coccorullo I, Speranza V, and Titomanlio G. Progress in Polymer Science 2005;30(12):1185-1222. doi:10.1016/j.progpolymsci.2005.09.001
8. Coccorullo I, Pantani R, and Titomanlio G. Polymer 2003;44(1):307-318. doi:10.1016/S0032-3861(02)00762-0
9. Pantani R, Coccorullo I, Speranza V, and Titomanlio G. Polymer 2007;48(9):2778-2790. doi:10.1016/j.polymer.2007.03.007
10. Pantani R, Balzano L, and Peters GWM. Macromolecular Materials and Engineering 2012;297(1):60-67. doi:10.1002/mame.201100158
11. Liu Q, Sun X, Li H, and Yan S. Polymer 2013;54(17):4404-4421. doi:10.1016/j.polymer.2013.04.066
12. Ma Z, Balzano L, Portale G, and Peters GW. Polymer 2014;55(23):6140-6151. doi:10.1016/j.polymer.2014.09.039
13. Acierno S, Coppola S, and Grizzuti N. Journal of Rheology 2008;52(2):551-566. doi:10.1122/1.2829149
14. Tavichai O, Feng L, and Kamal MR. Polymer Engineering & Science 2006;46(10):1468-1475. doi:10.1002/pen.20608
15. Liedauer S, Eder G, Janeschitz-Kriegl H, Jerschow P, Geymayer W, and Ingolic E. International Polymer Processing 1993;8(3):236-244. doi:10.3139/217.930236

16. Kumaraswamy G, Issaian AM, and Kornfield JA. Macromolecules 1999;32(22):7537-7547. doi:10.1021/ma990772j
17. Devaux N, Monasse B, Haudin J-M, Moldenaers P, and Vermant J. Rheologica acta 2004;43(3):210-222. doi:10.1007/s00397-003-0333-8
18. Mykhaylyk OO, Chambon P, Impradice C, Fairclough JPA, Terrill NJ, and Ryan AJ. Macromolecules 2010;43(5):2389-2405. doi:10.1021/ma902495z
19. Tanner RI. Journal of non-newtonian fluid mechanics 2002;102(2):397-408. doi:10.1016/S0377-0257(01)00189-6
20. Steenbakkers RJ and Peters GW. Rheologica acta 2008;47(5-6):643-665. doi:10.1007/s00397-008-0273-4
21. Pantani R, Speranza V, and Titomanlio G. Journal of Rheology 2015;59(2):377-390. doi:10.1122/1.4906121
22. Peters GW, Balzano L, and Steenbakkers RJ. Flow-Induced Crystallization. Handbook of Polymer Crystallization, 2013. pp. 399-432. doi:10.1002/9781118541838.ch14
23. Somma E, Valentino O, Titomanlio G, and Iannirubertо G. Journal of Rheology 2007;51(5):987-1005. doi:10.1122/1.2771175
24. Acierno S and Grizzuti N. Journal of Rheology 2003;47(2):563-576. doi:10.1122/1.1545080
25. De Santis F and Pantani R. Journal of thermal analysis and calorimetry 2013;112(3):1481-1488. doi:10.1007/s10973-012-2732-5
26. Cascone A and Fulchiron R. Polymer testing 2011;30(7):760-764. doi:10.1016/j.polymertesting.2011.06.012
27. Lamberti G, Peters G, and Titomanlio G. International Polymer Processing 2007;22(3):303-310. doi:10.3139/217.2006
28. Coppola S, Balzano L, Gioffredi E, Maffettone PL, and Grizzuti N. Polymer 2004;45(10):3249-3256. doi:10.1016/j.polymer.2004.03.049
29. De Santis F, Lamberti G, Peters GW, and Brucato V. European polymer journal 2005;41(10):2297-2302. doi:10.1016/j.eurpolymj.2005.04.032
30. Lamberti G and De Santis F. Heat and mass transfer 2007;43(11):1143-1150. doi:10.1007/s00231-006-0199-2
31. De Santis F, Vietri AR, and Pantani R. Macromolecular Symposia 2006;234:7-12. doi:10.1002/masy.200650202
32. De Santis F, Pantani R, and Titomanlio G. Polymer 2016;90:102-110. doi:10.1016/j.polymer.2016.02.059
33. Pantani R. European polymer journal 2005;41(7):1484-1492. doi:10.1016/j.eurpolymj.2005.02.006
34. Pantani R, Speranza V, Sorrentino A, and Titomanlio G. Macromolecular Symposia 2002;185:293-307. doi:10.1002/1521-3900(200208)185:1<293::AID-MASY293>3.0.CO;2-8
35. Macosko CW. Rheology: Principles, Measurements, and Applications: Wiley-VCH, 1994.
36. Pantani R, Speranza V, and Titomanlio G. Rheologica acta 2012;51(11-12):1041-1050. doi:10.1007/s00397-012-0660-8
37. Pantani R, Coccorullo I, Volpe V, and Titomanlio G. Macromolecules 2010;43(21):9030-9038. doi:10.1021/ma101775h
38. Speranza V, Vietri U, and Pantani R. Macromolecular Research 2011;19(6):542-554. doi:10.1007/s13233-011-0610-9
39. Coccorullo I, Pantani R, and Titomanlio G. Macromolecules 2008;41(23):9214-9223. doi:10.1021/ma801524t